Research Paper

Seismic Behavior of Tall Buildings with End Shear Walls and Opening

Mehran Akhavan Salmassi[1], Ali Kheyroddin[2*] and Ali Hemmati[3]

1. Ph.D. Candidate of Structural Engineering, Seismic Geotechnical and High Performance Concrete Research Center, Department of Civil Engineering, Semnan Branch, Islamic Azad University, Semnan, Iran
2. Professor of Structural Engineering, Faculty of Civil Engineering, Semnan University, Iran, *Corresponding Author; email: kheyroddin@semnan.ac.ir
3. Assistant Professor of Structural Engineering Seismic Geotechnical and High Performance Concrete Research Center, Department of Civil Engineering, Semnan Branch, Islamic Azad University, Semnan, Iran

Received: 20/11/2022
Revised: 08/01/2023
Accepted: 22/01/2023

ABSTRACT

Today, many strategies have been proposed to improve the behavior of tall buildings under seismic load. Drifts, torsion, and structure period are essential parameters affecting high-rise building behavior. In addition, the stress concentration at the end wing of shear walls is another critical subject in high-rise buildings, which was resolved using end shear walls. The end shear wall connects the end of two shear walls in high-rise buildings without opening. In this study, a new end shear wall connects the end of shear walls in a high-rise building with regular openings (ESWO). Therefore, two 30-story RC buildings with and without end shear walls with opening were modeled by a nonlinear time history analysis under seismic load. The drift was decreased by 49% in a 30-story building with a new end shear wall. Moreover, the residual displacement of 30-story buildings with end shear walls with opening was decreased by 67%. The time history nonlinear analysis investigation indicated that the end shear walls with opening declined the maximum displacement by 62% in tall buildings by OpenSEES software. The reduction of the standard deviation of data increased the confinement in 30-story drifts in the X and Y directions by end shear walls with opening. Based on the results, the performance of the end shear walls with the opening was appropriate in the seismic behavior of high-rise buildings.

Keywords:
Reinforced concrete; Seismic behavior; Nonlinear time history analysis; End shear wall; Tall buildings

1. Introduction

The shear wall system in high-rise buildings includes some advantages and disadvantages. Increasing the stiffness of the building, preventing collapse, reducing damage, providing serviceability for high-rise buildings during earthquakes, and carrying gravity loads after many cracks are advantages. On the other hand, the disadvantages are a shear failure, uplift force by incorrectly estimating the number and improper placement of walls, displacement, and deformation due to axial force. Studies have sought to improve the performance of high-rise buildings, such as the end shear wall without opening in the Kingdom Tower structure [1].

Stafford Smith and Abergel [2] investigated coupled and shear walls in high-rise buildings and used an equivalent single coupled wall, which resulted in some distribution in the coupled wall and shear walls. Wyatt and Best [3] found dynamic response in medium-high buildings under

wind loads and indicated that the high response levels were primarily a result of exposure to the site. In addition, Roberts and Yeung [4] studied the torsional properties of doubly symmetric core shear walls and confirmed that sidewall distortion could effectively reduce the torsional stiffness of sections. Chen et al. [5] conducted a nonlinear inelastic analysis in a structure with a thin wall and showed that the mentioned inelastic analysis is suitable for the inelastic behavior and ultimate strength of core-braced frames. Mendis [6] focused on the warping analysis of concrete cores and presented a simple method for estimating the longitudinal stresses on walls and header beam forces, especially for torsional-loaded concrete cores. Onu [7] evaluated the warping shear effect in a thin-walled core and showed an average warp-restrained torsion. A site effect was reported by Wen et al. [8] for high-rise shear walls subjected to near- and far-field excitations. Kim et al. [9] presented an efficient three-dimensional seismic analysis of shear walls in high-rise buildings and proposed a method with high-accuracy results and low computational time. Meftah et al. [10] examined high-rise, thin-walled buildings and presented a method for comparing them with the finite element method. Smith and Willford [11] studied the damped outrigger concept for high-rise buildings and showed that the mentioned concept reduced the section size of members.

Zhao and Astaneh-Asl [12] showed that the behavior of composite shear walls in seismic conditions led to an innovative system using smart structures technology. Esmaili et al. [13] investigated structural RC shear walls in high-rise buildings and obtained an optimal tower design after examining ductility levels in shear walls. Mortezaei and Kheyroddin [14] discussed the effect size in RC flanged shear walls and reported that the effect size is independent.

Moreover, Rahai and Hatami [15] evaluated the behavior of composite shear walls subjected to cyclic loading and showed that the middle beam rigidity connections do not significantly affect the behavior of the mentioned shear walls. Khatami and Kheyroddin [16] studied the effect of flange thickness on the nonlinear behavior of flanged shear walls and showed that the global behavior of flange under pressure is much more improved than tension. Hoenderkamp [17] assessed the influence of a single shear wall on a coupled shear wall in high-rise buildings and proposed a graphical method for the rapid evaluation of structural behavior.

Bozdogan and Duygu Ozturk [18] examined the vibration analysis of symmetric shear walls by the transfer matrix method and showed reasonable accuracy. Emsen and Aksogan [19] performed a static analysis on shear walls using a continuous connection method and proposed a practical approach for pre-design. Moragaspitiya et al. [20] developed a vibration method for bearing elements in RC buildings and offered an approximate method to add the effects of creep and shrinkage. A simplified wide-column model was innovated by other structural shear walls using the wall's energy dissipation and inelastic behavior [21]. Bhunia et al. [22] presented a conceptual design for shear walls and improved solutions to compare performance-based strategies. Wei et al. [23] studied mesh boundary motion by simulating wind effects and presented a method to focus on clustered boundary meshes for turbulent flow simulation. Kheyroddin et al. [24] investigated open and semi-open core wall systems in high-rise buildings and found that a closed section core in the last story leads to appropriate behavior of the previous quarter of structure height due to the analytical results in the last story. The thin RC walls and related seismic behavior showed that the ultimate displacement capacity and energy dissipation ability decline when the wall thickness is reduced by 25% [25]. Tang and Su [26] evaluated the gravity-induced shear force in RC walls on transfer structures and proposed remedial measures, such as increasing the depth of the transfer girders using late-cast slabs, segmented upper shear walls, and higher-grade concrete for critical regions. Beiraghi et al. [27] investigated the energy dissipation of tall core-wall structures with multi-plastic hinges under near- and far-fault excitations and showed that inelastic energy dissipation is significant at the base and above the mid-height of the wall.

Liu et al. [28] examined the shear lag effect of a T-shaped short-leg shear wall and found that

the numerical calculation and theatrical analysis are compatible. Welt et al. [29] studied the boundary element in RC walls and realized those boundary elements in axial compression are more extensive than in unconfined concrete. A formulation of the mixed beam and its warping were investigated for dynamic analysis of thin-walled structures, and the proposed model was analyzed by time history and modal methods [30]. Wang et al. [31] innovated precast concrete shear walls and used them in high-rise modular buildings for designing a lateral load-resisting system and reported suitable performance under lateral loads. Satriani et al. [32] evaluated the seismic performance of moment-resistant frames by fragility curve with and without shear walls. According to the results, the frame-shear wall structure had better performance with a lower damage probability than other structures. Ugalde and Lopez-Garcia [33] investigated the behavior of RC shear wall buildings under earthquake and showed that elastic analysis has limitations in reproducing the actual observed behavior without damage state.

According to Mahmoud [34], the top of the building structure is the most undesirable location for the sky bridge due to the dynamic responses of high-rise buildings connected horizontally at different heights under earthquake loads. On the other hand, Lacidogna et al. [35] evaluated diagrid systems coupled with closed- and open-section shear walls in high-rise buildings and realized that the inclination of the external diagonals significantly affected the relative stiffness. Jeong et al. [36] studied the seismic performance in high-rise buildings and showed that coupling beams included high-rise buildings' most vulnerable seismic loads. Afzali et al. [37] investigated seismic performance in RC shear walls in high-rise buildings with various frequencies and found that earthquake frequency content changes were suitable for two high-rise structures rather than shorter structures. Khademian et al. [38] assessed the structural damage detection of RC shear walls under earthquake and observed cooperative agreement in some curves, such as displacement and base shear curves, due to experimental and numerical programs. Badkoubeh and Massumi [39] focused on the vibration period for the seismic design of RC shear walls and realized that mechanical wall properties and geometry significantly affect the entire period of concrete SW buildings. Akbarzadeh et al. [40] investigated coupling beams considering seismic behavior in RC frames with a coupled shear wall. RC coupling shear walls with concrete and steel coupling beams possess an identical drift distribution over the height until the final displacement. Akhavan Salmassi et al. [41] studied end shear walls in tall buildings with torsional irregularity under wind load. The end shear walls were investigated in tall buildings using torsional irregularity under seismic load and linear static analysis and indicated the behavior improvement of structures subjected to seismic load [42]. In addition, a comparative study was conducted on tall buildings by outrigger, braced, and RC wall core and presented that the buildings with RC shear walls had lower residual displacement than those with the braced core. Others have examined the seismic behavior of RC structures with shear walls subjected to main-shock and post-shock seismic sequences. These studies presented one of the determinative parameters for structural behavior subjected to seismic sequences by the post-shock to main-shock PGA ratio [43].

Therefore, the end shear wall connects the end of two shear walls in tall buildings without opening. In this study, a new shear wall was connected to the end of shear walls in high-rise buildings using an end shear wall with regular openings (ESWO). Two 30-story buildings were modeled by OpenSEES with reinforced concrete frames with RC shear walls and ESWO systems under seismic load and analyzed using nonlinear time history analysis to investigate ESWO. The ESWO caused proper seismic performance in RC tall buildings by improving roof displacement, con-finement, and architecture.

2. Material and Methods

2.1. Mathematical Formulation

Torsion is one of the most critical parameters in shear walls in high-rise buildings. The shear wall systems are rigid at the core base and have torsions at the top. In Figure (1a), these walls are

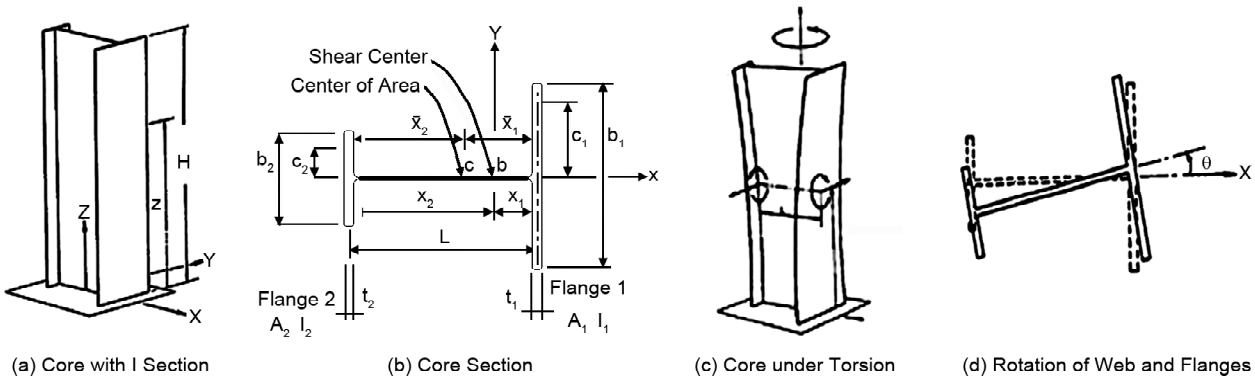

(a) Core with I Section (b) Core Section (c) Core under Torsion (d) Rotation of Web and Flanges

Figure 1. Simple cross-section, I [44].

symmetrical in the X and Y axes, assuming a simple cross-section I under the torsion of the eccentric ratio of 0.05, in which the warping effect is observed (ASCE7-16 (2017)) [44]. Z-axis and the wings rotate around the shear center, as well as the X- and vertical axes, respectively, by applying the torsion T above the Z-axis. In the moment effect, the slab sections revolve around the X-axis in different directions, and the plate sections are exited or warped from the plate. Smith and Coull [44] noted that the spin of the wings tolerates the torsion, which is equal to (see Figure (1)):

Figure (1b), $\bar{x}_1$, $\bar{x}_2, x_1$, and x_2 are the area and shear center (C and D points) as below:

$$\bar{x}_1 = \frac{A_2}{A_1 + A_2} L \qquad \bar{x}_2 = \frac{A_2}{A_1 + A_2} L \tag{1}$$

$$x_1 = \frac{I_2}{I_1 + I_2} L \qquad x_2 = \frac{I_2}{I_1 + I_2} L \tag{2}$$

Vlasov theory investigated torsion (Figures (1c) and (1d)), which is as follows:

$$T(z) = T_v(z) + T_w(z) \tag{3}$$

$T(z)$ and T_w represent torsion related to warping and torsion of shear flow, respectively. In addition, Figure (1c) shows shear related to flange moments 1 and 2 by Equations (4) and (5):

$$Q_1(z) = -EI_1 x_1 \frac{d^3\theta}{dz^3}(z) \tag{4}$$

$$Q_2(z) = -EI_2 x_2 \frac{d^3\theta}{dz^3}(z) \tag{5}$$

$$T_w(z) = Q_1(z)x_1 + Q_2(z)x_2 \tag{6}$$

$$T_w(z) = -EI_\omega \frac{d^3\theta}{dz^3}(z) \tag{7}$$

I_ω is geometric properties of section and nominated warping constant, which equals to:

$$I_\omega = I_1 x_1^2 + I_2 x_2^2 \tag{8}$$

$T_v(z)$ is tolerated by rotations in flanges as below:

$$T_v(z) = GI_1 \frac{d\theta}{dz}(z) \tag{9}$$

J_1 is the torsion constant of the section as follows:

$$J_1 = \frac{1}{3}\sum^{n} bt^3 \tag{10}$$

$$J_1 = \frac{b1t_1^3}{3} + \frac{b2t_2^3}{3} \tag{11}$$

GJ_1 expresses the torsional rigidity of the core by open section. The equation of torsion due to warping is given in Equation (12):

$$-EI_w \frac{d^3\theta}{dz^3}(z) + GJ_1 \frac{d\theta}{dz}(z) = T \tag{12}$$

On the other hand, the second moment $B(z)$ and vertical tension of the wall at distance c from the neutral axis are equal to:

$$B(z) = M(z)L \tag{13}$$

$$\sigma(c,z) = \frac{M(z)c}{I} \tag{14}$$

The warping theory of uniform core under

torsion, Vlasov theory (Equations (3), (7), and (9)), and their differential equations are presented as follows:

L presents the vertical distance of two flanges. $m(z)$ or wide torsion along the wide axis is equal to:

$$-m(z)=\frac{d_T}{d_z} \tag{15}$$

α is the position of the shear center differential equation for core warping torsion as shown in Equation (17):

$$\alpha^2=\frac{GJ}{EI_\omega} \tag{16}$$

$$\frac{d^4\theta}{dz^4}(z)-\alpha^2\frac{d^2\theta}{dz^2}(z)=\frac{m(z)}{EI_\omega} \tag{17}$$

Applying boundary conditions and solving the torsion of the core under $m(z)$ is obtained in Equation (17):

$$\theta(z)=\frac{mH}{EI_\omega}\left\{\frac{1}{(\alpha H)^4}\left[\frac{(\alpha H\sin h\,\alpha H+1)}{\cos h\,\alpha H}\times\right.\right.$$
$$(\cos h\,\alpha z-1)-\alpha H\sin h\,\alpha z+$$
$$\left.\left.(\alpha H)^2\left[\frac{z}{H}-\frac{1}{2}\left(\frac{z}{H}\right)^2\right]\right]\right\} \tag{18}$$

$$\alpha H=H\sqrt{\frac{GI}{EI_\omega}} \tag{19}$$

$$\alpha H=H\left(\frac{z}{H}\right) \tag{20}$$

Where two parameters of αH and z/H are dimensionless [43]. Warping tensions are mentioned as follows:

$$B(z)=-EI_\omega\frac{d^2\theta}{dz^2}(z) \tag{21}$$

$B(z)$ is the second moment, which specifies the core height. $\omega(s)$ is the principle of sectoral coordinate in the section. The tension distribution in height is shown below:

$$\sigma(s,z)=\frac{B(z)\omega(s)}{I_\omega} \tag{22}$$

Equation (22) indicates that the ESWO performs properly when some parameters are improved, considering stress reduction by the device.

2.2 Specifications of Structures and Material

A total of two 30-story buildings were modeled by ETABS software with and without ESWO to investigate the ESWO behavior (Figure 2). In addition, the seismic behavior was analyzed in three dimensions, including the reinforced concrete moment frame and shear wall. Dead and live loads were assumed as 170 and 200 (kg/m^2), respectively based on ASCE-16. The floor was reinforced concrete slab, and the connections of columns and shear walls were rigid at the base. The frames' spans and the floors' heights were 7 and 4 m, respectively.

Moreover, υ, f_c, and f_y were 0.15, 50 (MPa), and 400 (MPa), respectively. A nonlinear time history analysis was performed using OpenSEES after ETABS software determined the frame sections.

Figure (2a) shows the shear walls on C, D, 3, and 4 axes. In addition, the ESWO in A, F, 1, and D axes in Figures (2b), (2c), and (2d) indicated the typical frame elevation of the structure with ESWO and its detail.

As shown in Table (1) (the specifications of the concrete frames of the models), the 30-story buildings represent high-rise structures.

Tables (2) and (3) represent the buildings and section specifications.

These structures are subjected to seismic analysis after modeling and then analyzed.

Table 1. Concrete frames models.

Label	Description	Range	
		Name	Stories
CMF_1	Concrete Moment Frame without ESWO	High-Rise	30
CMF_2	Concrete Moment Frame with ESWO	High-Rise	30

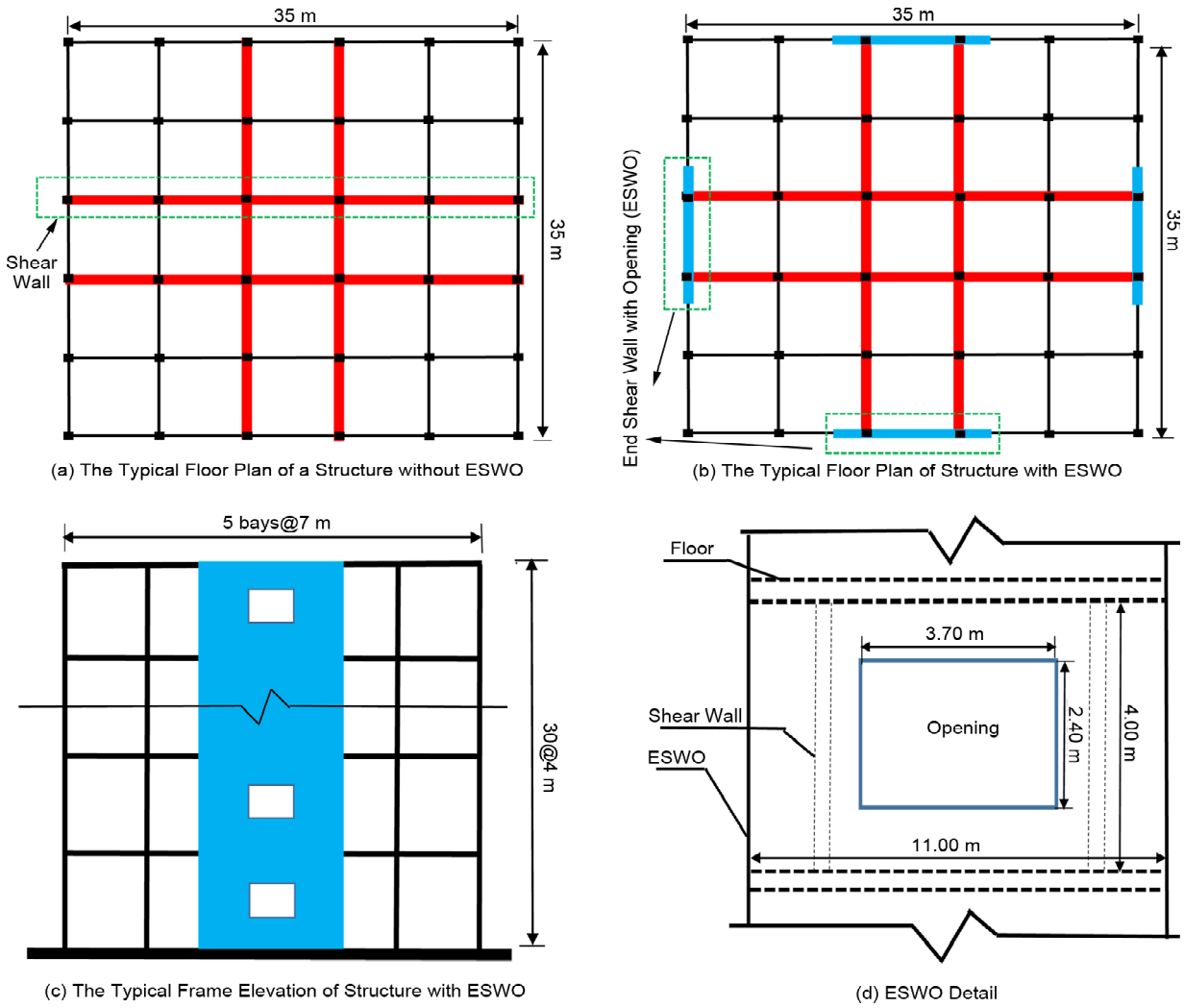

Figure 2. 30-story models.

Table 2. Building specifications.

Name	H (m)	A (m^2)	Plan Dimensions (m×m)	Story
Building1 without ESWO	120	36750	35×35	30
Building 2 with ESWO	120	36750	35×35	30

Table 3. Section specifications.

Label	Dimension	Rebar
Beam	St1-30: (0.5) m wide×(0.7) m deep	8Φ20- Stirrup Φ14@10cm
Column	St1-15:(1.20) m×(1.20) m, St16-30:(1.00) m×(1.00) m	36Φ32 - 36Φ32 – Stirrup Φ14@15cm
Shear Wall	St1-30:(35) m long×(0.5) m thick	Φ28@10cm-Stirrup Φ14@25cm
ESWO	St1-30:(11) m long×(0.5) m thick	Φ28@10cm-Stirrup Φ14@25cm
Slab	St1-30:(0.15) m thick	Φ10@10cm

2.3. Simulation of the Structures

The 30-Story structures were analyzed by linear static analysis and determined the section properties. The mentioned structure was simulated by OpenSEES for more investigations and nonlinear time history analyses. Three records were required to apply the structures due to nonlinear time history analysis.

On the other hand, the multi-layer shell element model was applied for shear walls using the "ShellMITC4" command related to the multi-layer shell element model. The mentioned command subdivided the shear wall into a sufficient number of layers. According to the dimensions and

distribution of reinforcing bars, Figure (3) [45] indicates the different material properties and multi-layer shell elements. Given the physical location and direction of the bars smeared into some orthotropic layers, the layer thickness stresses were assumed to be consistent with those at the mid-surface (Figure 4) [45].

Table (4) lists the specifications of the records, which are considered far-field by site class D. On the other hand, acceleration time, response acceleration time, and the spectra response of records are indicated in Figures (5) and (6), respectively.

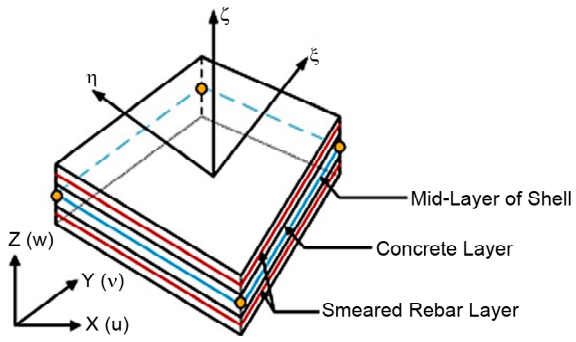

Figure 3. Multi-layer shell element [45].

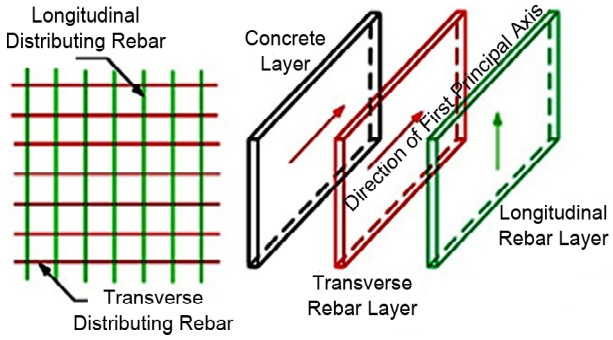

Figure 4. Distribution of rebar layer [45].

Table 4. Specifications of the records.

Event	Station	Year	M_w	d (km)	PGA_{max} (g)	PGA_{max}(g) / PGV_{max}(cm/sec)
Loma Prieta	Gilroy Array #4	1989	6.93	14.34	0.419	1.040
Morgan Hill	Gilory Array #4	1984	6.19	11.54	0.349	2.010
Northwest China-03	Jaishi	1997	6.1	17.73	0.3	1.558

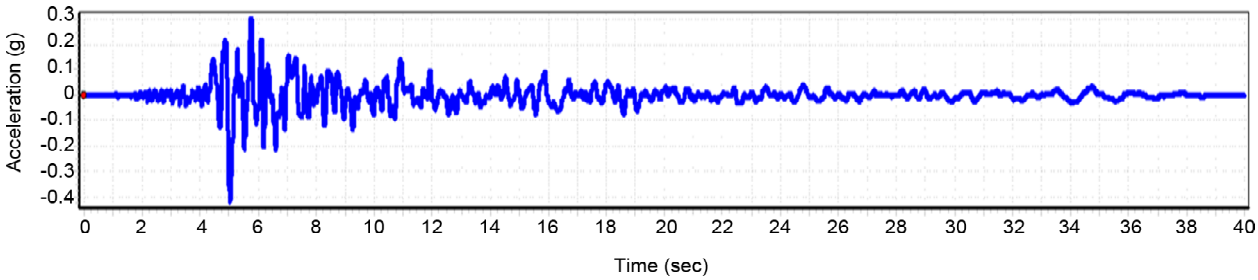

(a) Loma Prieta, Acceleration-Time

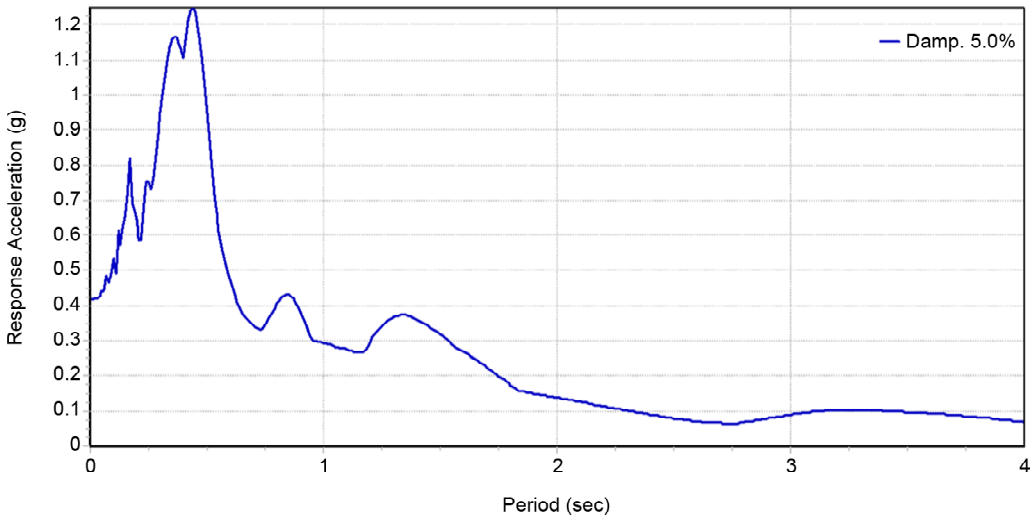

(b) Loma Prieta, Response Acceleration-Time

Figure 5. The Acceleration-time and Response acceleration- time graphs of records.

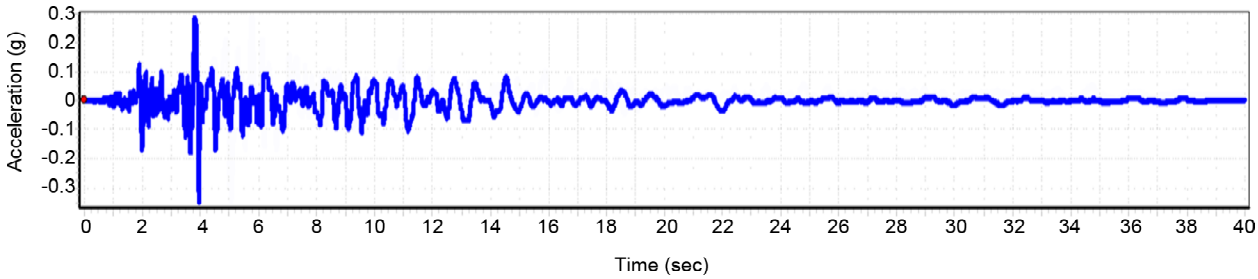

(c) Morgan Hill, Acceleration-Time

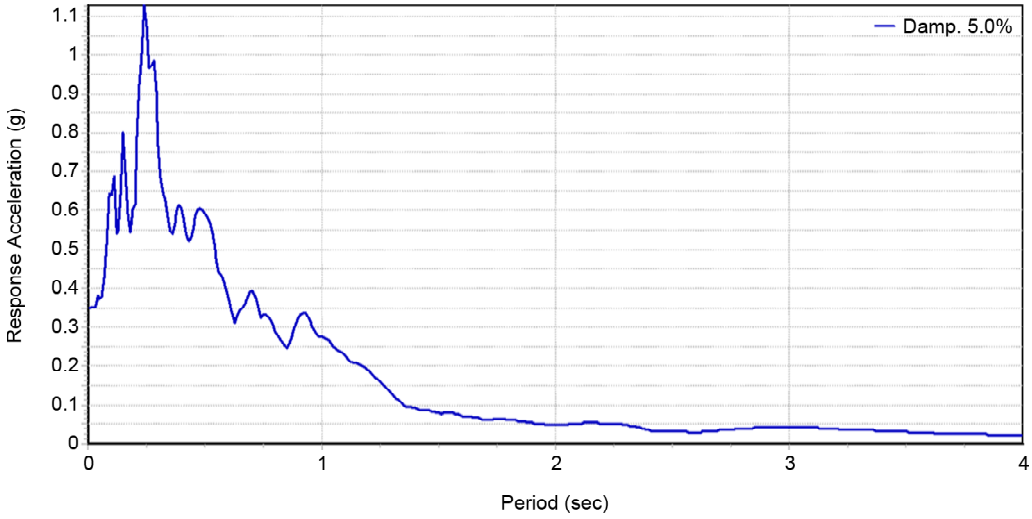

(d) Morgan Hill, Response Acceleration-Time

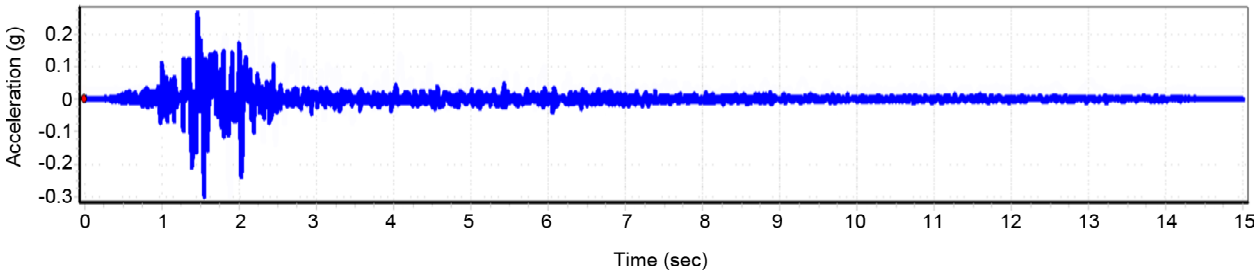

(e) Northwest China-03, Acceleration-Time

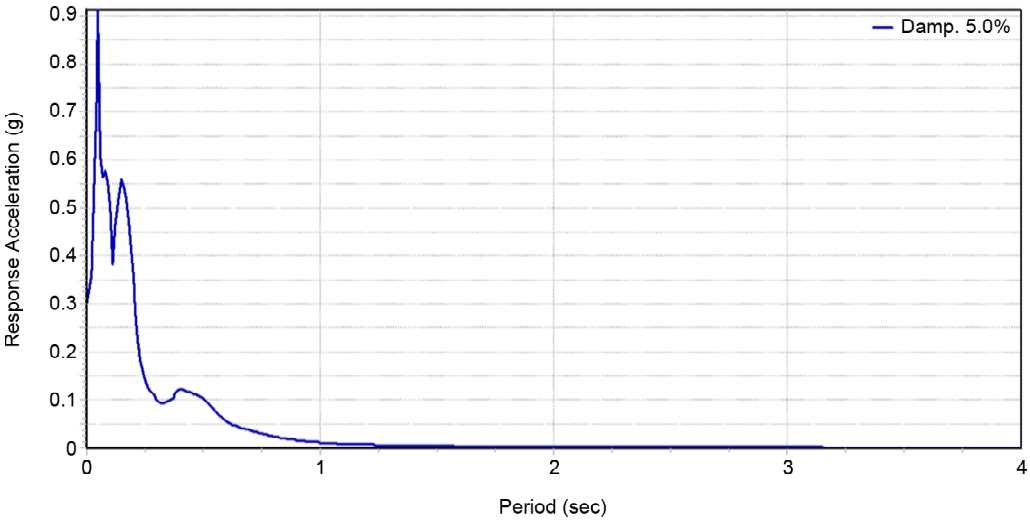

(f) Northwest China-03, Response Acceleration-Time

Figure 5. Continue.

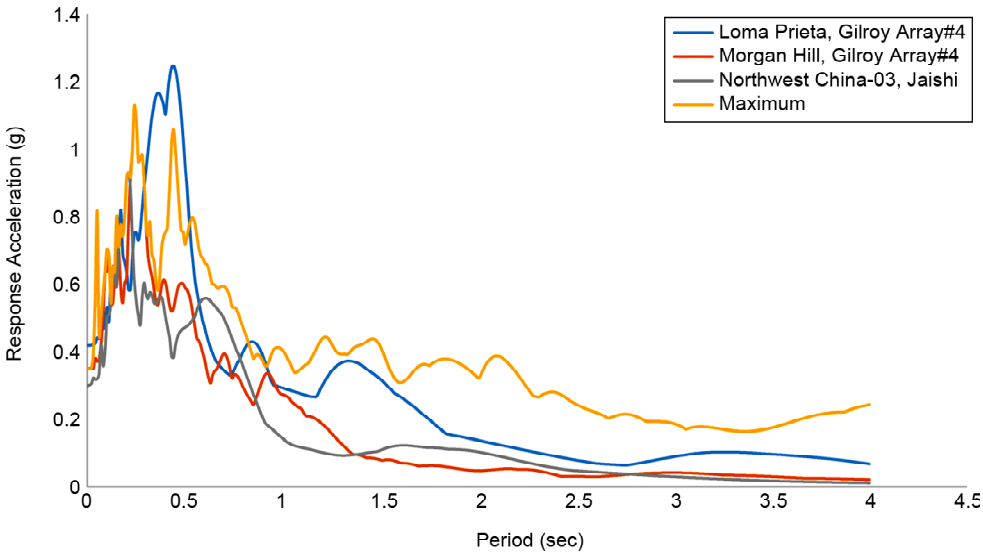

Figure 6. The spectra response of records.

A nonlinear time analysis of structures requires verification in the following.

2.3.1. Verification

In this study, the OpenSEES algorithms are validated on a four-story RC flexural frame studied by Parra et al. [46] in Figure (7a). In Figure (7b) and Table (5), the maximum base shear/W (%) of Parra et al. [46] and simulation ratios are 10.5% and 11.1%, respectively.

Table 5. TVerification results.

Analysis Type	(Maximum Base Shear/W) (%)
Article Analysis	10.5
Verification Analysis	11.1

The verification deviation was 5%, and the comparison of curves showed the appropriate performance of the algorithm by OpenSEES.

Validation for the frame with open shear wall according to Mamdouh et al. [47] in Figures (8a) and (8b) is as follows:

Lateral displacement was measured using linear variable differential transducers (LVDT), and the relationship between the applied lateral loads and the horizontal displacement at the top of the specified tested shear walls before strengthening is shown in Figure (8a). It is evident from the figures that the load-deflection curves of all specimens follow the same pattern. Before the ultimate load and the failure stage, the elastic load-deflection curve held steady up until the cracking load. Because of a loss of stiffness and rigidity, the slope of the curve dropped at all three of the places evaluated as the opening size grew larger. The ability of the applied GFRP sheets to regulate stress redistribution and fracture propagation resulted in an increase in curve slope and lateral load capacity following the strengthening process. It was found that the displacement capacity of the walls with the aperture was lower than that of the reference wall without opening, but that

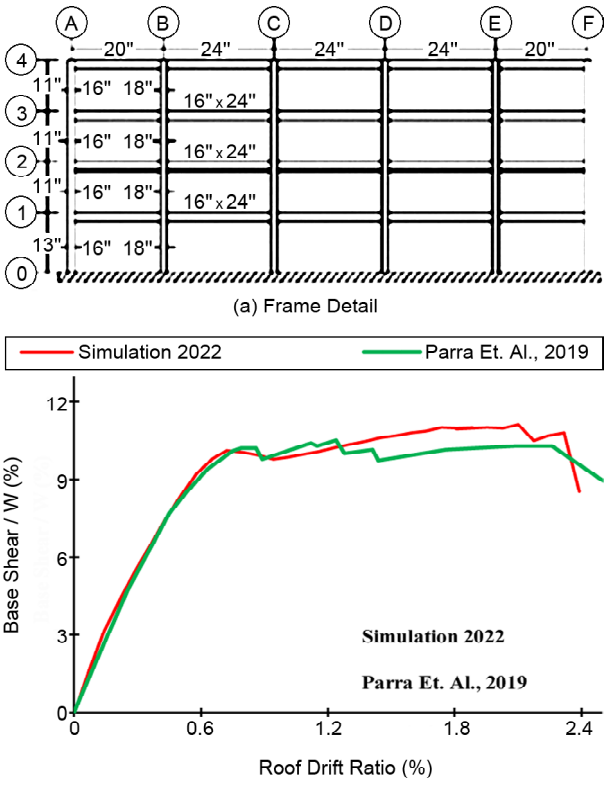

Figure 7. The verification frame and results.

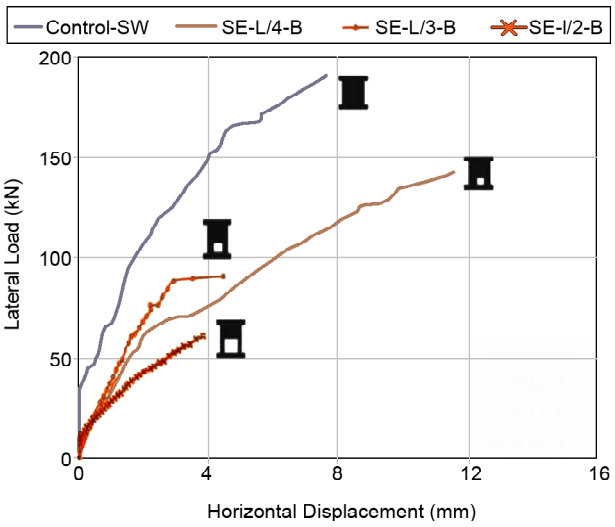

(a) Lateral Load Versus Lateral Displacement Curves for Groups (**B**) before Strenghtening

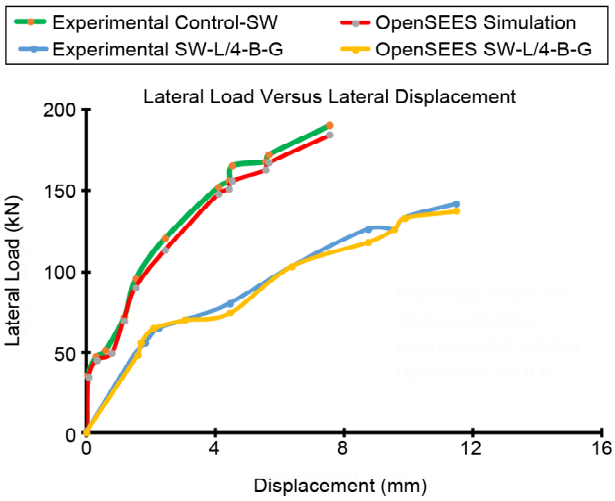

(b) Lateral load versus lateral displacement curves for groups (**B**) and OpenSEES simulation

Figure 8. The detail of the verification specimen and OpenSEES simulation.

this was mitigated by the use of GFRPs around the opening, resulting in a considerably more forgiving load-displacement response.

3. Result and Discussion

The two 30-story structures were modeled with and without ESWO in three nonlinear time history analysis records. The structure is modeled in three dimensions The time history analysis is based on FEMA-P695. Three components of the record have been applied based on Table (3) and the maximum values has been considered. The drift ratio is one of the significant parameters in seismic behavior in tall buildings. Based on Figure (9), the drift ratios are calculated for this purpose.

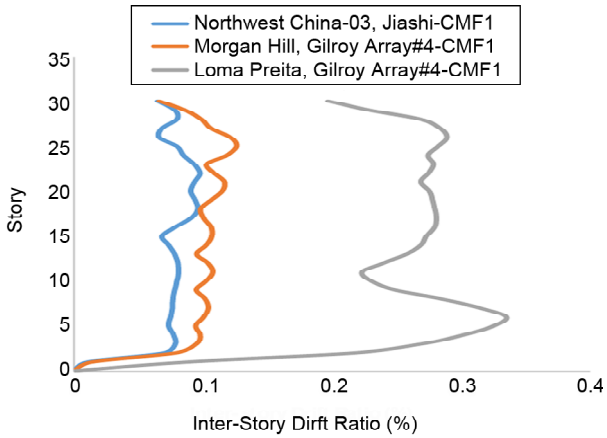

(a) The Inter-Story Drift Ratios (%) of Records Based on the Story in CMF1

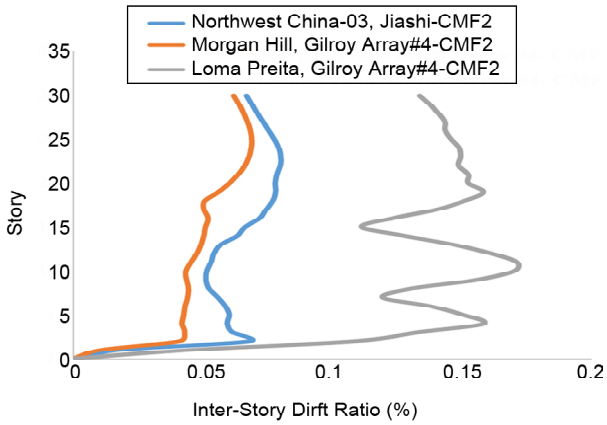

(b) The Inter-Story Drift Ratios (%) of Records Based on the Story in CMF2

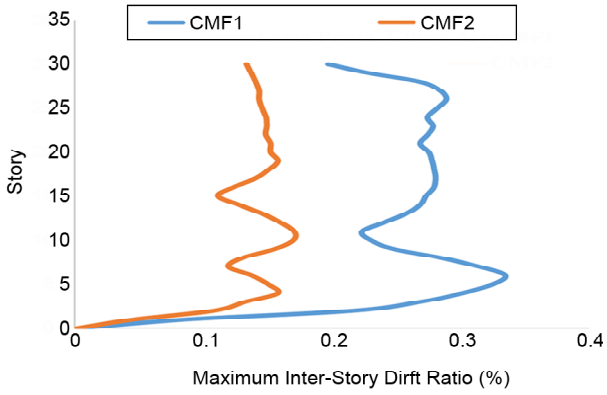

(c) Comparison of Maximum Inter-Story Drift Ratios (%) of Records Based on the Story in CMF1 and CMF2

Figure 9. The drift ratios (%) based on the story in CMF1 and CMF2.

Figure (9a) shows the inter-story drift ratios for records based on the story of CMF1. As observed, the orange, blue, and gray colors belonged to Morgan hill, Northwest China, and Loma Prieta records, respectively. The minimum inter-story ratio occurred at 8.75E-04, 1.41E-04, and 1.07E-04 in Loma Prieta, Morgan hill, and Northwest China records at the first level, respectively.

The maximum drift ratios equal 3.35E-03, 1.26E-03, and 9.72E-04 in Loma Prieta, Morgan hill, and Northwest China records at six-, 25-, and 22-stories, respectively, despite some fluctuation from one to 13-stories.

The inter-story drift ratios of records are shown in Figure (9b), which is based on the story of CMF2. The minimum inter-story ratio was observed at 4.09E-04, 1.14E-04, and 1.89E-04 in Loma Prieta, Morgan hill, and Northwest China records at the first level, respectively. There were gradual fluctuations in the parameters mentioned above from one to 13 stories in three records. The maximum inter-story drift ratios were obtained at 6.92E-04 and 8.03E-04 in Morgan Hill and Northwest China records. Some initial fluctuation resulted in 1.71E-03 in the Loma Prieta record at ten levels.

The inter-story drift ratio based on the story of CMF1 and CMF2 is presented in Figure (9c). The mentioned inter-story drift ratio was obtained from the maximum inter-story drift ratios of three records in CMF1 and CMF2 in every story. In CMF1 and CMF2, the minimum inter-story drift ratios were 8.75E-04 and 4.63E-04 at first level, respectively. In addition, the maximum parameters mentioned above were 3.35E-03 and 1.71E-03 at the six and eleven levels of CMF1 and CMF2 by some fluctuations, respectively.

Moreover, Figure (10) indicates that the displacement time history of the Loma Prieta records in the CMF1 and CMF2 structures at the roof level. The CMF1 graph showed an increasing behavior from zero to 15.9588s by a maximum displacement of -23.7981cm, which declined to -6.6564cm, and the ESWO caused a rough uniform behavior. The maximum displacement was presented at 8.8321 cm in 1211 s, and the residual displacement of CMF2 was equal to -2.13275 cm.

The maximum inter-story drift was at eleven levels of CMF2 under the Loma Prieta record. In Figure (11), the drift graph under the Loma Prieta record indicates a deeper exploration of ESWO's effects by nonlinear time history analysis.

The drift ratios had more concentration in CMF2 than in CMF1. Figure (11a) demonstrates the drift in X- based on the Y-direction of CMF1 and CMF2 under Loma Prieta. Therefore, SPSS software was used to analyze data to provide more accurate information about the Figure mentioned above. There were significant differences in the proportion of CMF1 and CMF2 at box plot outputs. On the other hand, there are some data at the top and bottom of the box plot in Figure (11b) for CMF1 to express the scattered data at the top of the box plot in Figure (11c) for CMF2. In addition, the CMf2 box plot indicated a lower domain as much as -0.001 and 0.0015 than CMF1 by more domains from -0.003 to 0.003. CMF2 had a greater concentration of data in the X-direction than CMF1. Furthermore, Figures (11d) and Figure (11e) show that CMF2 has a lower domain (-5.0 E-04 and 7.5 E-04) than CMF1 by more domains in -0.002 and 0.002 in the Y direction.

Thus, ESWO's suitable performance increased the confinement of data in CMF2 by presenting a greater concentration than that in CMF1.

Table (6) shows the drift outputs of X and Y directions in CMF1 and CMF2 structures under Loma Prieta by SPSS software. The standard deviations were significantly lower in CMF2 to CMF1 in two directions with a brief review.

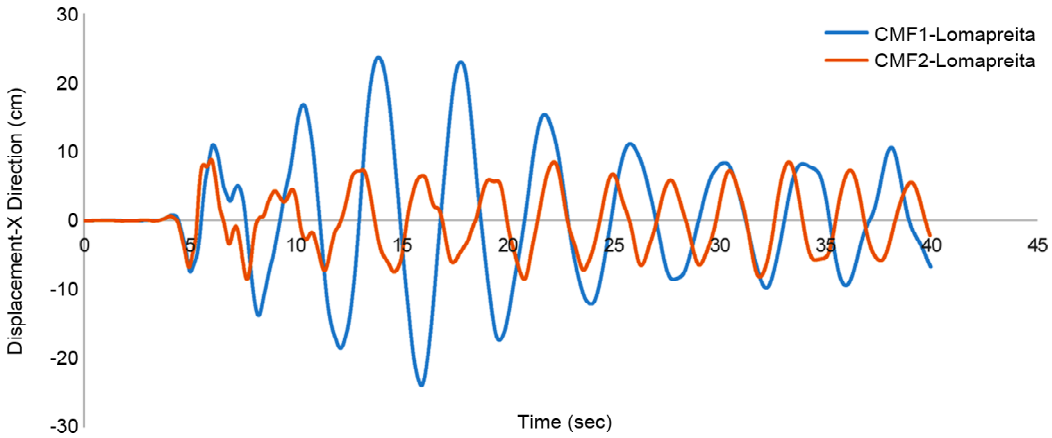

Figure 10. The displacement Time history of roof under Loma Prieta record.

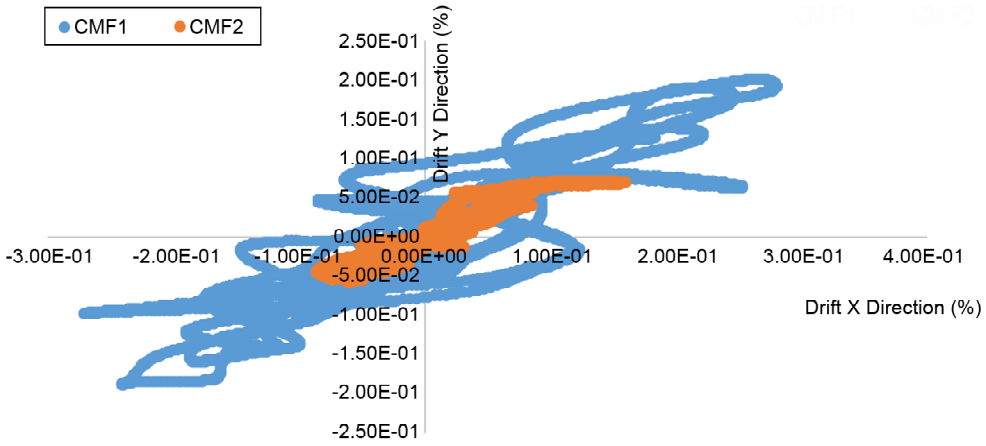

(a) The Drift (%) in X Direction Based on the Drift (%) in Y Direction CMF1 and CMF2 under Loma Prieta

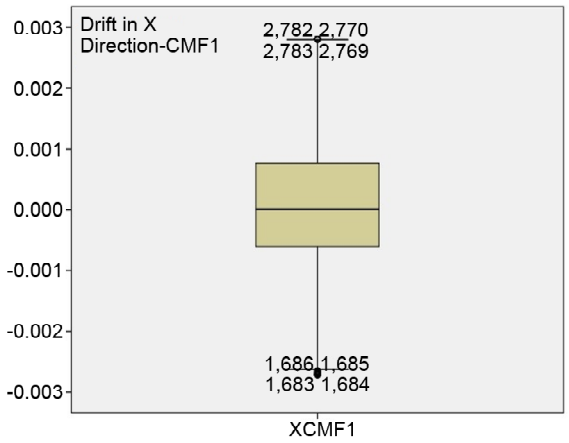

(b) The Box Plot of Drift in X Direction CMF1 in Loma Prieta

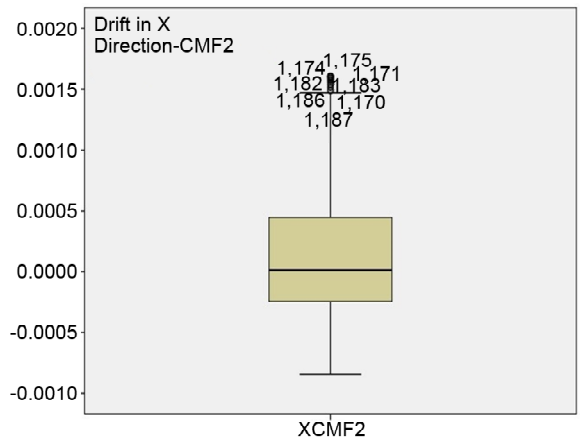

(c) The Box Plot of Drift in X Direction CMF2 in Loma Prieta

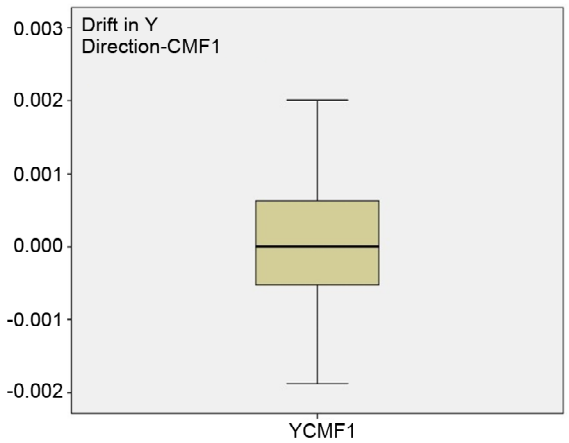

(c) The Box Plot of Drift in Y Direction CMF1 in Loma Prieta

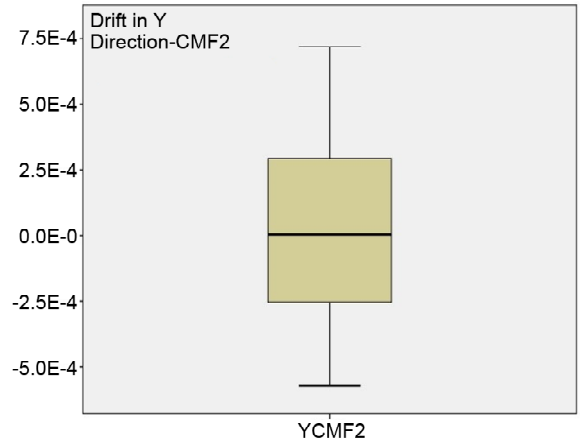

(d) The Box Plot of Drift in Y Direction CMF2 in Loma Prieta

Figure 11. The drifts and boxes plot of CMF1 and CMF2 in X and Y directions in Loma Prieta.

In addition, the number of standard deviations of "Drift X-direction CMF1 Loma Prieta" and "Drift X-direction CMF2 Loma Prieta" were presented obviously by 0.00101 and 0.00042, respectively. In addition, the standard deviations changed from 0.00079 to 0.00032 in "Drift Y direction CMF1 Loma Prieta" and "Drift Y direction CMF2 Loma Prieta" respectively.

The standard deviation values were expressed with less dispersion of drift data in CMF2 in X and Y directions under excitation than in CMF1.

According to the study, new end shear walls improved the seismic behavior of tall buildings in terms of structure and architecture.

Table 6. The statistics of standard deviation.

	XCMF1	YCMF1	XCMF2	YCMF2
Std. Deviation	0.00101	0.00079	0.00042	0.00032

4. Conclusion

Modeling of two 30-story buildings with and without ESWO structures was performed by OpenSEES to investigate the seismic behavior of the new end shear wall (end shear wall with regular openings or ESWO). In addition, the data were analyzed by SPSS software, and the following results were obtained:

- The mentioned structures were subjected to Northwest China, Morgan Hill, and Loma Prieta records due to nonlinear time history analysis in 30-story structures. The inter-story drift ratio was one of the significant parameters for investigating tall building structures. The related graph drew into three sections. The inter-story drift ratio was based on 30 stories with and without ESWO, and other maximum inter-story drift ratios were compared to the two previous graphs. The results indicated that the maximum drift decreased as much as 49% in 30 stories by ESWO, considering some fluctuation.
- Time history displacement graphs showed nonlinear time-history analysis results for both systems, which presented the roof displacement based on time in the X-direction. Immediate and substantial differences were observed in time history displacement graphs of 30 stories with end ESWO, and the maximum displacement decreased by 62% in 30-story structures with ESWO.
- As a result of performing efficient ESWO in maximum displacement, residual displacement of ESWO was demonstrated. In this regard, the residual displacement of the roof was presented in the X-direction under three records. The ESWO improved the residual displacement by as much as 67%, considering the residual displacement values.
- The excellent structural efficiency and ESWO increased the confinement in tall buildings by box plots outputs. Based on the results, the standard deviation of data declined by 58 and 59% in 30-story drift by ESWO in the X- and Y-directions, respectively.

Notation and Symbols

The following symbols are used in this paper:

A: area of the plan
$B(z)$: second moment
E: young module
f_c': concrete comprehensive strength
f_y': yield strength of steel
GJ: torsional rigidity of the core
H: height of the structure
I: inertia moment
J_1: torsion constant
L: vertical distance of two wings
$M(z)$: wide torsion along the wide axis
T: torsion
$T_w(z)$: torsion associated with the warping
$T_v(z)$: torsion associated with the shear currents
α: position of the shear center differential equation for core warping
υ: poison coefficient
ρ: concrete reinforced ratio
$\sigma(c, z)$: vertical tension of the wall at a distance c from the neutral axis
$\sigma(s, z)$: distribution of tension in height (z)
$\omega(s)$: principle sectoral coordinates

References

1. Leventis, G., Poeppel, A., and Syngros, K. (2015) *From Supertall to Megatall: Analysis and Design of the Kingdom Tower Piled RaftNo Title*. 44-52.

2. Stafford Smith, B. and Abergel, D.P. (1983) Approximate analysis of high-rise structures comprising coupled walls and shear walls. *Building and Environment*, **18**(1-2), 91-96, https://doi.org/10.1016/0360-1323(83)90022-7.

3. Wyatt, T.A. and Best, G. (1984) Case study of the dynamic response of a medium-height building to wind-gust loading. *Engineering Structures*, 6(4), 256-261, https://doi.org/10.1016/0141-0296(84)90021-X.

4. Roberts, T.M. and Yeung, K.W. (1992) Bending

and torsion of doubly symmetric core shear walls. *Thin-Walled Structures*, **14**(5), 395-410, https://doi.org/10.1016/0263-8231(92)90010-T.

5. Chen, H. Liew, J.Y.R., and Shanmugam, N.E. (2000) Nonlinear inelastic analysis of building frames with thin-walled cores. *Thin-Walled Structures*, **37**(3), 189-205, https://doi.org/10.1016/S0263-8231(00)00016-1.

6. Mendis, P. (2001) Warping analysis of concrete cores. *Structural Design of Tall Buildings*, **10**(1), 43-52, http://dx.doi.org/10.1002/tal.160.

7. Onu, G. (1990) Inclusion of warping shear effect in the thin-walled core element for multistory building. *Computers & Structures*, **35**(2), 75-182, https://doi.org/10.1016/0045-7949(90)90335-Y.

8. Wen, Z.P., Hu, Y.X., and Chau, K.T. (2002) Site effect on the vulnerability of high-rise shear wall buildings under near and far field earthquakes. *Soil Dynamics and Earthquake Engineering*, **22**(9-12), 1175-1182, https://doi.org/10.1016/S0267-7261(02)00145-8.

9. Kim, H.S., Lee, D.G., and Kim, C.K. (2005) Efficient three-dimensional seismic analysis of a high-rise building structure with shear walls. *Engineering Structures*, **27**(6), 963-976, https://doi.org/10.1016/j.engstruct.2005.02.006.

10. Meftah, S.A., Tounsi, A., and El Abbas, A.B. (2007) A simplified approach for the seismic calculation of a tall building braced by shear walls and thin-walled open section structures. *Engineering Structures*, **29**(10), 2576-2585, https://doi.org/10.1016/j.engstruct.2006.12.014.

11. Smith, R.J. and Willford, M.R. (2007) The damped outrigger concept for tall buildings. *The Structural Design of Tall and Special Buildings*, **16**(4), 501-517, https://doi.org/10.1002/tal.413.

12. Zhao, Q. and Astaneh-Asl, A. (2007) Seismic behavior of composite shear wall systems and application of smart structures technology. *International Journal of Steel Structures*, **7**(7), 69-75.

13. Esmaili, O., Epackachi, S., Samadzad, M., and Mirghaderi, S.R. (2008) Study of structural RC shear wall system in a 56-story RC tall building. *The 14th World Conference on Earthquake Engineering*, Beijing, China, October.

14. Mortezaei, A. and Kheyroddin, A. (2009) Size effects in reinforced concrete flanged shear walls. *International Journal of Civil Engineering*, **7**(1), 27-40.

15. Rahai, A. and Hatami, F. (2009) Evaluation of composite shear wall behavior under cyclic loadings. *Journal of Constructional Steel Research*, **65**(7), 1528-1537, https://doi.org/10.1016/j.jcsr.2009.03.011.

16. Khatami, S.M. and Kheyroddin, A. (2011) The Effect of flange thickness on the behavior of flanged. section shear walls. *Procedia Engineering*, **14**, 2994-3000, https://doi.org/10.1016/j.proeng.2011.07.377.

17. Hoenderkamp, J.C.D. (2011) The influence of single shear walls on the behaviour of coupled shear walls in high-rise structures. *Procedia Engineering*, **14**, 1816-1824, https://doi.org/10.1016/j.proeng.2011.07.228.

18. Bozdogan, K.B. and Duygu Ozturk, A.D. (2012) Vibration analysis of asymmetric shear wall - frame structures using the transfer matrix method. *Iranian Journal of Science and Technology - Transactions of Civil Engineering*, **36**(C1), 1-12, https://doi.org/10.22099/IJSTC.2012.641.

19. Emsen, E. and Aksogan, O. (2012) Static analysis of non-planar coupled shear walls with stepwise changes in geometrical properties using continuous connection method. *Thin-Walled Structures*, **56**, 21-32, https://doi.org/10.1016/j.tws.2012.03.006.

20. Moragaspitiya, H.N., Thambiratnam, D.P., Perera, N.J., and Chan, T.H.T. (2013) Development of a vibration-based method to update axial shortening of vertical load bearing elements in reinforced concrete. https://doi.org/10.1016/j.engstruct.2012.07.010.

21. Encina, J. and de la Llera, J.C. (2013) A simplified model for the analysis of free plan buildings using a wide-column model.

Engineering Structures, **56**, 738-748.

22. Bhunia, D., Prakash, V., and Pandey, A.D. (2013) *A Conceptual Design Approach of Coupled Shear Walls*. ISRN Civil Engineering, 1-28.

23. Wei, D. Spence, S.M.J., Kareem, A., and Jemcov, A. (2014) A structured mesh boundary motion approach for simulating wind effects on bluff bodies with changing boundaries. *Journal of Wind Engineering and Industrial Aerodynamics*, **126**, 118-131, https://doi.org/10.1016/j.jweia.2014.01.008.

24. Kheyroddin, A., Abdollahzadeh, D., and Mastali, M. (2014) Improvement of an open and semi-open core wall system in tall buildings by the closing of the core section in the last story. *International Journal of Advanced Structural Engineering*, **6**(3), 1-12.

25. Hube, M.A., Marihuén, A., de la Llera, J.C., and Stojadinovic, B. (2014) Seismic behavior of slender reinforced concrete walls. *Engineering Structures*, **80**, 377-388, https://doi.org/10.1016/j.engstruct.2014.09.014.

26. Tang, T.O. and Su, R.K.L. (2015) Gravity-induced shear force in reinforced concrete walls above transfer structures. *Proceedings of the Institution of Civil Engineers. Structures and Buildings*, **168**(1), 40-55. https://doi.org/10.1680/stbu.13.00092.

27. Beiraghi, H., Kheyroddin, A., and Kafi, M.A. (2016) Energy dissipation of tall core-wall structures with multi-plastic hinges subjected to forward directivity near-fault and far-fault earthquakes. *The Structural Design of Tall and Special Buildings*, **25**(15), 801-820, https://doi.org/10.1002/tal.1284.

28. Liu, C. et al (2017) Research on the shear lag effect of T-shaped short-leg shear wall. *Periodica Polytechnica Civil Engineering*, **61**(3), 602-610, http://dx.doi.org/10.3311/PPci.9491.

29. Welt, T.S., Lehman, D.E., and LaFave, J.M. (2018) Boundary elements are detailing in special concrete structural walls. *ACI Structural Journal*, **115**(3), 635-647, https://doi.org/10.14359/51701278.

30. Di Re, P., Addessi, D., and Paolone, A. (2019) Mixed beam formulation with cross-section warping for dynamic analysis of thin-walled structures. *Thin-Walled Structures*, **141**, 554-575, https://doi.org/10.1016/j.tws.2019.04.014.

31. Wang, Z., Pan, W., and Zhang, Z. (2020) High-rise modular buildings with innovative precast concrete shear walls as a lateral force resisting system. *Structures*, **26**, 39-53, https://doi.org/10.1016/j.istruc.2020.04.006.

32. Satriani, L., Sangadji, S., Purwanto, E., and Kristiawan, S.A. (2017) Assessing seismic performance of moment resisting frame and frame-shear wall system using seismic fragility curve. *Procedia Engineering*, **171**, 1069-1076.

33. Ugalde, D. and Lopez-Garcia, D. (2017) Behavior of reinforced concrete shear wall buildings subjected to a large earthquake. *Procedia Engineering*, **199**, 3582- 3587, https://doi.org/10.1016/j.proeng.2017.09.524.

34. Mahmoud, S. (2019) Horizontally connected high-rise buildings under earthquake loadings. *Ain Shams Engineering Journal*, **10**(1), 227-241, https://doi.org/10.1016/j.asej.2018.12.007.

35. Lacidogna, G., Nitti, G., Scaramozzino, D., and Carpinteri, A. (2020) A Diagrid systems coupled with closed- and open-section shear walls: Optimization of geometrical characteristics in tall buildings. *Procedia Manufacturing*, **44**, 402-409, https://doi.org/10.1016/j.promfg.2020.02.277.

36. Jeong, S.Y., Kang, T.H.K., Yoon, J.K., and Klemencic, C.R. (2020) Seismic performance evaluation of a tall building: practical modeling of surrounding basement structures. *Journal of Building Engineering*, **31**, 1-13, https://doi.org/10.1016/j.jobe.2020.101420.

37. Afzali, A., Mortezaei, A., and Kheyroddin, A. (2017) Seismic performance of high-rise RC shear wall buildings subjected to ground motions with various frequency contents. *Civil Engineering Journal*, **3**(8), 568-584, https://doi.org/10.28991/cej-2017-00000113.

38. Khademian, F., Naderpour, H., and Sharbatdar,

M.K. (2019) Structural damage detection of reinforced concrete shear walls subject to consequent earthquakes. *SN Applied Sciences*, **92**, https://doi.org/10.1007/s42452-019-1899-9.

39. Badkoubeh, A. and Massumi, A. (2017) Fundamental period of vibration for seismic design of concrete shear wall buildings. *Scientia Iranica*, **24**(3), 1010-1016, https://dx.doi.org/10.24200/sci.2017.4084.

40. Akbarzadeh Bengara, H., and Mohammadalipour Askib, R. (2017) Effect of steel and concrete coupling beams on seismic behavior of RC frame accompanied with coupled shear walls. *Scientia Iranica*, **24**(5), 2227-2241, https://dx.doi.org/10.24200/sci.2017.4159.

41. Akhavan Salmassi, M., Kheyroddin, A., and Hemmati, A. (2020) Seismic behavior of end walls in RC tall buildings with torsional irregularity. *Magazine of Civil Engineering*, **97**(5), 64-76, https://doi.org/10.18720/MCE.97.7.

42. Samadi, M. and Jahan, N. (2021) Comparative study on the effect of outrigger on seismic response of tall buildings with braced and RC wall core. I: Optimum level and examining modal response spectrum analysis reliability. *Tall and Special Buildings*, **30**(8), https://doi.org/10.1002/tal.1848.

43. Karimzade Soureshjani, O., and Massumi, A. (2022) Seismic behavior of RC moment resisting structures with concrete shear wall under mainshock-aftershock seismic sequences. *Bulletin of Earthquake Engineering*, **20**(2), 1-28, https://link.springer.com/article/10.1007%2Fs10518-021-01291-x.

44. Smith B.S, and Coull A (1991). *Tall Building Structures Analysis and Design*. John Wiley & Sons Press, New York, NY, USA.

45. Lu, X., Xie, L., Guan, Guang, H., Huang, Y., and Lu, X. (2015) A shear wall element for non-linear seismic analysis of super-tall buildings using OpenSEES. *Finite Elem. Anal*, **98**, 14-25, https://doi.org/10.1016/j.finel.2015.01.006.

46. Parra, P.F., Arteta, C.A., and Moehle, J.P. (2019) Modeling criteria of the older non-ductile concrete frame-wall buildings. *Bulletin of Earthquake Engineering*, **3**(17), 6591-6620, https://doi.org/10.1007/s10518-019-00697-y.

47. Mamdouh, H., Zenhom, N., Hasabo, M., Deifalla, A.F., and Salman, A. (2022) Performance of strengthened, reinforced concrete shear walls with opening. *Sustainability*, **14**(21), 1-32, https://doi.org/10.3390/su142114366.